

shows that the one-electron theory may not be capable of obtaining the correct magnitude of interband absorption in alkali metals. A similar conclusion was previously reached¹¹ for Al. There r_s (the mean inter-electronic spacing in Bohr units) is 2.0 and the calculated absorption was three times smaller than that observed. In Na we have $r_s=3.96$ and the calculated absorption appears to be at least ten times smaller than observed. Possibly the anomalously large interband absorption indicates breakdown of the one-electron theory at short wavelengths. This breakdown could also lead to the observed resonance behavior. Because interband absorption refers to fixed momentum transfers $\mathbf{q}=\mathbf{k}-\mathbf{k}'=\mathbf{K}$, rather than a range of momentum transfer (as would arise in resonance formation), it may

¹¹ H. Ehrenreich, H. R. Philipp, and B. Segall, Phys. Rev. **132**, 1918 (1963).

form a suitable starting point for theoretical research in the intermediate density regime $r_s \gtrsim 1$.

Note added in proof. Further de Haas-Van Alphen experiments on Na by M. J. G. Lee tentatively indicate a somewhat larger value of $|V_{110}|$ than quoted in this paper (the new value is slightly above our upper limit of 0.2 eV). While further work is expected to add a second significant figure to this result, we do not believe that this slightly larger value will alter the conclusions of this paper. We are grateful to Dr. D. Shoenberg for permission to mention Lee's preliminary results.

ACKNOWLEDGMENT

I would like to thank Professor J. C. Phillips for suggesting this problem, as well as for his guidance throughout its execution.

Resistivity Recovery of Dilute Alloys of Silver, Copper, and Gold, Proton-Irradiated at 80°K*

D. A. GRENNING AND J. S. KOEHLER

Department of Physics and Materials Research Laboratory, University of Illinois, Urbana, Illinois

(Received 29 November 1965)

Ag-Be, Ag-Li, Cu-Be, Au-Mg, and Au-Al were irradiated by 12-MeV protons at 80°K. High-resolution isochronals were then obtained from -130 to 90°C and activation energies were determined every 10°C using the change-of-slope method. The order associated with the reaction kinetics was determined at temperatures appropriate for the various annealing peaks by fitting 240-min isothermal anneals to first or second order. The recovery of the silver and copper alloys showed remarkable similarity to pure silver and copper, but the gold-alloy recovery was markedly altered as compared with pure gold. Activation energies for the stage-III defect in silver, copper, and gold alloys were found to be 0.64, 0.71, and 0.70 eV, respectively. The copper and silver alloys had a small first-order recovery stage near the low-temperature side of the main stage-III annealing peak. The main stage-III peak obeyed second-order kinetics in all cases. In the gold alloys the stage-III recovery was composed of a main second-order annealing peak with a small second-order annealing peak on each side of the main peak. These annealing results have been fitted to the various models for the recovery of damage, and some conclusions are drawn.

I. INTRODUCTION

AT present the basic nature of the annealing processes occurring in stage I (10 to 100°K) is reasonably well understood. In both fcc and bcc metals a series of close interstitial vacancy pairs recombine.¹⁻³ At a temperature a little above temperatures associated with these close pairs, one has demonstrated long-range migration of an interstitial in copper and aluminum.²⁻⁵

The geometrical arrangement of atoms constituting the interstitial defect which migrates in stage I is still being discussed.

Gold appears to be an anomalous material. The close-pair annealing peaks in copper and silver as seen by Palmer, Magnuson, and Koehler¹ in stage I are remarkably similar. However, Ward and Kauffman⁶ and later Bauer, DeFord, Koehler, and Kauffman⁷ found a very complex annealing spectrum for gold in stage I. Koehler and Leibfried⁸ have attempted to explain the difference by supposing that the interstitial structure in gold differs from that existing in copper and silver.

* This research was supported in part by the U. S. Atomic Energy Commission Contract No. AT(11-1)-1198.

¹ G. D. Magnuson, W. Palmer, and J. S. Koehler, Phys. Rev. **109**, 1990 (1958).

² J. W. Corbett, R. B. Smith, and R. M. Walter, Phys. Rev. **114**, 1452 (1959).

³ T. G. Nilan and A. V. Granato, Phys. Rev. **137**, 1233 (1965).

⁴ M. L. Swanson and G. R. Piercy, Can. J. Phys. **42**, 1605 (1964).

⁵ D. Thompson, T. Blewitt, and D. Holmes, J. Appl. Phys. **28**, 742 (1957).

⁶ J. B. Ward and J. W. Kauffman, Phys. Rev. **123**, 90 (1960).

⁷ W. Bauer, J. W. DeFord, J. S. Koehler, and J. W. Kauffman, Phys. Rev. **128**, 1497 (1962).

⁸ J. S. Koehler and G. Leibfried, J. Phys. Soc. Japan **18**, Suppl. III, 266 (1963).

There are fewer data and less agreement concerning the basic processes which occur in stage III (-40 to $+50^\circ\text{C}$). The three models suggested to date are:

(a) Interstitials migrate in stage I and recombine with vacancies or cluster. The vacancies remaining after stage I migrate in stage III.

(b) Two kinds of interstitials are produced during irradiation. One, a metastable interstitial which migrates in stage I; the second, a stable interstitial which migrates in stage III.

(c) Interstitials migrate in stage I and di-interstitials migrate in stage III.

The present experiments were undertaken in an attempt to decide between the above alternatives. Blewitt and co-workers⁹ in a set of valuable experiments discovered that impurity atoms having small closed shells, which go into solution in substitutional positions, are very effective in preventing the annealing associated with stage I. Copper containing 0.1% beryllium retains about half of the resistivity increment which would normally anneal in stage I up to a temperature above 200°K . In copper containing 0.1% silicon, the stage I damage is retained to about 150°K . Copper containing 0.1% nickel or zinc showed no important difference from pure copper. The only previous experiment in which stage-III annealing of dilute alloys was carefully examined were experiments by Sosin and Rachal¹⁰ and by Federighi and co-workers¹¹ on aluminum alloys. Unfortunately they used only impurities having large core size, and there is a good reason for believing that their influence differs from that of small core impurities.

One would expect (see discussion for details) substitutional impurities of small core size to trap the stage-I interstitial, as the above experimenters have observed. The purpose of the experiment, therefore, was to observe the way in which stage III is affected by the presence of the trapped stage-I interstitial. From this it was hoped that conclusions might be drawn about the type of defects responsible for stage-III recovery.

II. APPARATUS AND PROCEDURE

The specimens used were in the form of cold-rolled strips 5 mil by 1 mm by 15 cm long. The samples were mounted in aluminum blocks as described by Dworschak *et al.*¹² with the slight modification that the proton beam is perpendicular to the flat face of the foil. The protons then had to penetrate two 5-mil samples at most. The energy loss of the 12- to 13-MeV protons used was calculated to be, for 10 mil of copper, silver, or

gold, 5.6, 5.7, and 8.3 MeV, respectively, but there was no way of experimentally determining this in our arrangement.

In each sample block a thermocouple was mounted consisting of a copper strip duplicating one leg of a sample, with a thin constantan wire soldered to the center of the leg. With this dummy sample the temperature of the sample was monitored using a Leeds and Northrup microvolt amplifier and recorder. Recording the temperature rise of the dummy sample at the beginning of each anneal gave a criteria for starting the annealing times, since for low-temperature anneals (-130 to -100°C) the rise time from liquid-nitrogen to the bath temperature was about 3 min. Corrections to the annealing time were made using these records as described in Appendix I. For no single anneal did the correction exceed 15 sec. This was due to the fact that the correction times were very insensitive to time at temperatures more than 15°C below the bath temperature. Also, in order to compensate for the rise time, the starting time began at a temperature about 2°C below the desired temperature.

The temperature of the samples was monitored during irradiation. The beam intensity was thus regulated to keep the temperature of the dummy sample below 110°K . This turned out to be a current of roughly 0.2×10^{-6} A/cm². After irradiation the samples were stored in liquid nitrogen until they were annealed.

The cryostat in which the samples were irradiated was described by Herschbach and Witt.¹² The Faraday cup mounted on the cryostat had nine probes placed uniformly over the beam area. Uniformity of the beam was maintained within $\pm 15\%$ of the average value on all probes. The cryostat for annealing the specimens was that used by Dworschak, Herschbach, and Koehler.¹³

All resistance measurements except those during irradiation were made at liquid-helium temperature, using a current of $0.9000x \pm 0.00001$ A through the samples with simultaneous voltage readings across the samples. The x in the fifth zero position indicates that the value of the current was not known absolutely to six places, but could be reproduced to six places. To measure the current, a 1- Ω standard resistor was placed in series with the samples. A K-3 potentiometer in conjunction with a Leeds and Northrup null detector was then placed across the 1- Ω standard. The current source was a Regatron Power Supply built by Electronic Measurements Company of Eatontown, New Jersey. It was used as a voltage source for four variable 10- Ω resistors in series with current ratings of 10 A apiece in order to prevent heating and thus drifting of the current. The potential across the samples was read with a Rubicon six-dial potentiometer in conjunction with a photoelectric galvanometer.

⁹ T. H. Blewitt, R. R. Coltman, C. E. Klabunde, and T. S. Nogge, *J. Appl. Phys.* **28**, 639 (1957).

¹⁰ A. Sosin and L. H. Rachal, *Phys. Rev.* **130**, 2238 (1963).

¹¹ S. Ceresara, T. Federighi, and F. Pieragostini, *Phil. Mag.* **10**, 893 (1964).

¹² F. Dworschak, K. Herschbach, and F. Witt, *Rev. Sci. Instr.* **35**, 46 (1964).

¹³ F. Dworschak, K. Herschbach, and J. S. Koehler, *Phys. Rev.* **133**, A293 (1963).

TABLE I. Composition of alloys studied. All numbers in atomic parts per million.

Alloy	Solute	Background impurities													Total background impurity	
		Al	Ca	Cu	Au	Fe	Pb	Mg	Si	Sn	Ni	V	In	Tl		Ag
Ag+Be	110	1.2	1.3	1.7	1.1	1.0	0.16	2.2	7.7	0.27						16.7
Ag+Be	440		<0.27	0.52	0.55	0.97		0.44	0.77	0.27						3.79
Ag+Be	1400		0.54	1.7	1.1	0.97		0.88	0.38			1.1				14.6
Ag+Li	190	0.8	<0.27	0.51		0.97		4.4	12					6.8		25.2
Ag+Li	12 000	0.4	0.54		2.7	0.97	0.26	2.2	0.77	0.27			0.47			8.58
Au+Mg	405		0.97	0.93		1.8			3.4						0.91	8
Au+Mg	1100	7.3	15	6.2					14		6.7		1.7		3.7	54.4
Au+Al	110		1.5	3.1		1.1		4.1	14						3.7	27.5
Au+Al	1500		2.5	3.1		1.8		4.1	21		3.4	1.4		4.1	1.8	43.2
Cu+Be	290		0.79		0.32	0.11	0.031	0.52	1.1		1.1				0.06	4.04
Cu+Be	1900	0.24	7.9		0.65	0.23	0.031	7.8	16		1.1	0.12			0.06	34.0

III. PREPARATION OF SAMPLES

The primary concern in choosing the impurities for this experiment was the size of their closed shell core in relation to copper, silver, and gold; ($r_{Be}=0.32$, $r_{Mg}=0.65$, $r_{Al}=0.50$, $r_{Cu}=0.96$, $r_{Ag}=1.26$, $r_{Au}=1.37$ Å)¹⁴ since previous work by Blewitt and co-workers has shown this to be the main factor in suppressing stage I.⁹ All of the alloy concentrations are given in atomic percent. Cominco Products, Inc., of Spokane, Washington, supplied the alloys along with spectroscopic analysis of the major and background impurities as listed in Table I. The Ag-Be and Ag-Li systems were extremely difficult to fabricate. The low-concentration Ag-Li system eventually proved unreliable both before and after irradiation and so only a small amount of data was taken on it.

It would be best to have annealed all of the alloys in order to remove dislocations before irradiation, but this was found to be impossible in some of the alloys. Figure 1 shows how the resistance ratio, defined in Eq. (1) of Appendix II, for the Ag-Be system varies as a function of the temperature of the anneal, where all anneals are for four hours.

In order to discover what was happening to the beryllium in Ag+0.011 Be, a simple experiment was performed. First, 50 g of Ag+0.011 Be, in the form of strips described above, were etched. The etch consisted of a bath of acetone, then methyl alcohol, and finally a solution of one part hydrogen peroxide and three parts ammonium hydroxide with a final rinse in distilled water. The Ag+0.011 Be samples were then annealed for 4 h at 225°C in a vacuum furnace. The vacuum was always better than 5×10^{-6} mm of mercury. Half of the Ag+0.011 Be was then etched as above in order to remove the surface. Both halves were then assayed by Cominco for beryllium content. Also the resistance ratio of the annealed Ag+0.011 Be was measured to be 192 when it had been 84 before anneal. The assay stated that

the Ag+0.011 Be annealed, but not etched after anneal had 0.0096 at.% beryllium and that the Ag+0.011 Be etched before and after anneal had 0.0072 at.% beryllium. This indicated that some beryllium had migrated to the surface during anneal and was etched away. Using these assays along with the resistivity of beryllium in silver, (determined in Appendix II and shown in Table II to be $\delta\rho_{Be \text{ in Ag}}=0.90 \times 10^{-6} \Omega \text{ cm/at.}\%$) and Eq. (1) of Appendix II, it was found that in order to arrive at a ratio of 192, the beryllium could not be uniformly distributed throughout the lattice. In order to get the best fit to a ratio of 192 and the assays, the most probable explanation is that some of the beryllium agglomerates at grain boundaries and dislocations while some migrates to the surface becoming oxidized and is removed by the second etch.

In the case of Cu+0.07 Be it was again found that the resistance ratio increases as a function of the annealing temperature as shown in Fig. 1. By annealing Cu+0.19 Be at 500°C for 4 h, the resistance ratio was changed on the average from 13 to 20 indicating that about 0.06 at.% of beryllium was removed leaving the percent of beryllium at about 0.13 at.%. The same experiment was performed on Cu+0.07 Be as described above for Ag+0.011 Be, the only exception being that an etch of nitric acid and the KCN solution was used. It was again

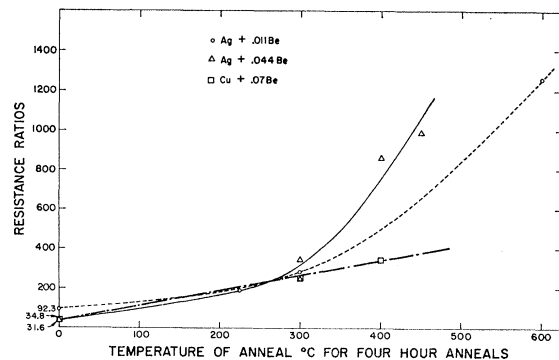


Fig. 1. Resistance ratio versus annealing temperature.

¹⁴ C. Kittel in *Introduction to Solid State Physics* (John Wiley & Sons, Inc., New York, 1956), 2nd ed., p. 81.

TABLE II. Alloy resistivity data. All values are calculated using Linde's data (Ref. 16).

Alloy as assayed (at.%)	Annealing procedure	Calculated background resistivity $10^{-9} \Omega \text{ cm}$	Calculated solute resistivity $10^{-9} \Omega \text{ cm}$	Calculated resistance ratio	Experimental resistance ratio	Calculated $\mu\Omega/(\text{at.}\%)$ $\delta\rho$ $(\delta\rho)_{av}$
Ag+0.011 Be	None	6.1			91.6	0.95
Ag+0.044 Be	None	1.4			31.6	1.08
Ag+0.14 Be	None	3.3			16.5	0.67
Ag+0.019 Li	None	14.9			54.6	0.63
Ag+1.2 Li	None	1.8			2.69	0.74
Au+0.04 Mg	500°C, 4 h	3.5	52	37.7	43.8	0.90
Au+0.11 Mg	500°C, 4 h	12.2	147	13.8	14.6	
Au+0.011 Al	500°C, 4 h	9.6	20.5	68.8	59.6	
Au+0.15 Al	500°C, 4 h	10.3	273.5	8.18	7.67	
Cu+0.029 Be	None	0.80	18.0	83.6	34.9	
Cu+0.19 Be	None	7.7	117.7	13.3	13	
Cu+0.19 Be	300°C, 4 h	7.7	117.7	13.3	20.4	

found that some beryllium was being trapped at the surface and some in the bulk of the lattice. Thus it was concluded that Cu+0.19 Be would be annealed but not Cu+0.07 Be, because the anneal would reduce the beryllium content so much that effective trapping of irradiation damage might not occur. In Cu+0.19 Be the beryllium content remained relatively high after the anneal.

The Au-Mg and Au-Al systems were all etched in aqua regia and annealed at 500°C in a vacuum of at least 5×10^{-6} mm of mercury for 4 h. Since the resistance ratios measured after these anneals were in good agreement with what would be expected, using Eq. (II.1) in Appendix II for the assayed impurity levels, it was felt that the slight amount of aluminum and magnesium agglomerated was not important in comparison to the removal of cold work.

The Ag-Li alloys never showed much reliability.

IV. DATA

A. The Resistance Ratios of the Samples

A total of 34 samples were mounted in 17 blocks, there being three samples per alloy plus an extra Ag+0.14 Be sample. The calculated resistivity due to

background impurities and the solute atoms, along with the calculated and experimental resistance ratios, are given in Table II. In general, there is good agreement between the calculated and experimental resistance ratios, indicating reliability of the alloy, except in the case of Cu+0.029 Be. Since six separate evaluations of the resistance ratio were made, all of which fell within 34.9 ± 2.0 , it is assumed that the assay is incorrect for Cu+0.029 Be. Using this resistance ratio and Linde's data,¹⁵ one finds that there is 0.07 Be present, so that this alloy is to be referred to as Cu+0.07 Be. There were no data available on the resistivity of beryllium or lithium in silver, so it has been determined, as described in Appendix II and shown in Table II, to be relatively consistent in each of the alloys.

B. Production of Damage in the Samples

Irradiation was started using 13-MeV protons, but the cyclotron operated poorly at this energy so that after irradiating a few samples, the energy was decreased to 12 MeV. In Table III, Dworschak, Herschbach, and Koehler's¹⁸ production rate for pure copper, silver, and gold bombarded with 10-MeV protons at 80°K is compared to the present author's production rates for

TABLE III. Production of damage in the samples. Note that in 10 mil of copper, silver, and gold the energy depreciation for protons with an initial energy of 12 to 13 MeV is 5.6, 5.7, and 8.3 MeV, respectively.

Material	Initial energy of protons MeV	Average production rate $10^{-9} \Omega \text{ cm}/(10^{15}/\text{cm}^2)$	Material	Initial energy of protons MeV	Average production rate $10^{-9} \Omega \text{ cm}/(10^{15}/\text{cm}^2)$
Ag	10	1.01	Au	10	1.86
Ag+0.011 Be	13.2	$1.37 \pm 50\%$	Au+0.04 Mg	13.2	$3.65 \pm 50\%$
Ag+0.044 Be	13.2	$2.49 \pm 50\%$	Au+0.11 Mg	13.2	$4.32 \pm 50\%$
Ag+0.14 Be	12.4	$1.94 \pm 50\%$	Au+0.011 Al	12.4	$7.07 \pm 50\%$
Ag+0.011 Li	12.4	$2.14 \pm 50\%$	Au+0.15 Al	12.4	$7.62 \pm 50\%$
Ag+1.2 Li	12.4	$2.43 \pm 50\%$	Cu	10.0	0.438
			Cu+0.07 Be	12.4	$1.15 \pm 50\%$
			Cu+0.19 Be	12.4	$3.24 \pm 50\%$

¹⁵ A. N. Gerritsen, in *Handbuch der Physik*, edited by S. Flügge (Springer-Verlag, Berlin, 1956), Vol. XIX, p. 210.

12- and 13-MeV protons. It is apparent from the large production rates for the alloys at 80°K that a good deal of stage I is being trapped.

Because of the large energy loss described earlier, a comparison of damage production in the alloys relative to pure metals will be uncertain to within $\pm 35\%$. Also, because of the design of the Faraday cup in this experiment, the error in counting charge is probably about $\pm 15\%$, yielding a total uncertainty of $\pm 50\%$ in the rate of production reported in Table III.

C. Isochronal Annealing Study

Isochronal anneals were taken for 10 min every 5°K to see whether there was any extraordinary behavior in the alloyed materials as compared with pure materials. Surprisingly, the annealing peaks found in the alloys were almost identical to those seen in pure materials even though large amounts of stage-I damage had been trapped in the alloys. This data is illustrated in Figs. 2 through 11 by plotting the percent recovery versus temperature. The percent recovery is defined as 100 times the resistivity decrease divided by the total resistivity introduced by irradiation.

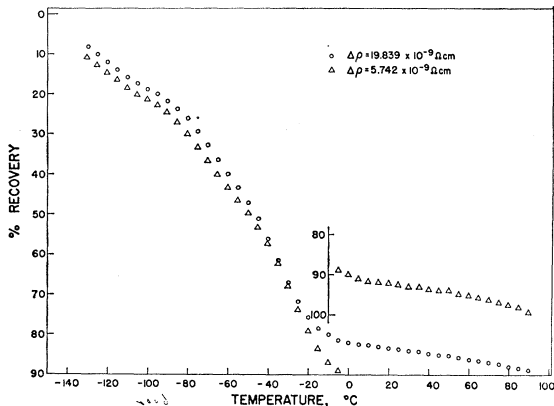


FIG. 2. Isochronals of Ag+0.011 Be, percent recovery versus temperature.

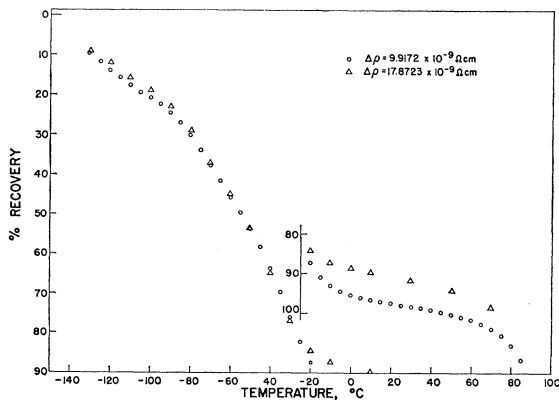


FIG. 3. Isochronals of Ag+0.044 Be, percent recovery versus temperature.

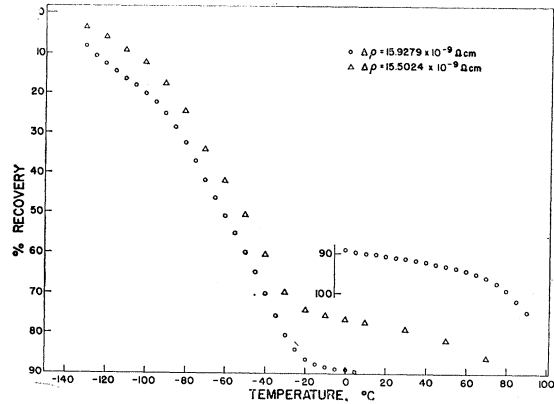


FIG. 4. Isochronals of Ag+0.14 Be, percent recovery versus temperature.

It must be noted that in several of the alloys the percent recovery was more than 100%. This only occurred in the unannealed alloys and the percent

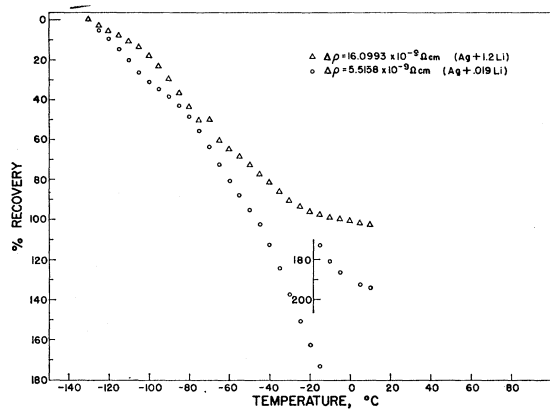


FIG. 5. Isochronals of Ag+0.019 Li and Ag+1.2 Li.

recovery only went above 100% near room temperature. This occurred then because defects present before irradiation were being eliminated to some extent above

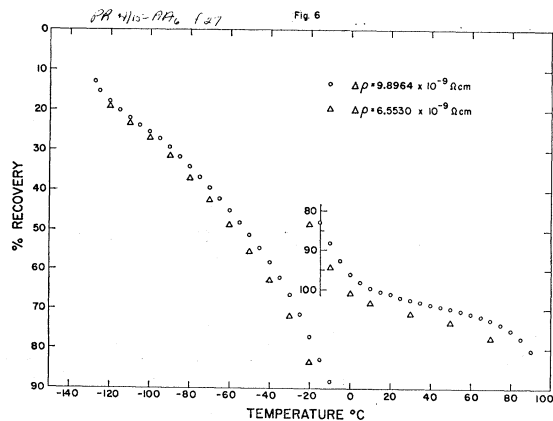


FIG. 6. Isochronals of Cu+0.07 Be, percent recovery versus temperature.

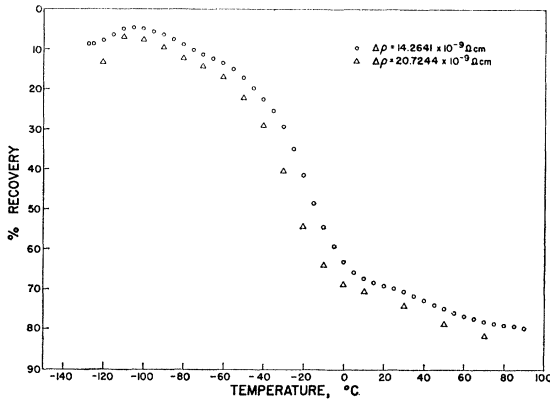


FIG. 7. Isochronals of Cu+0.19 Be, percent recovery versus temperature.

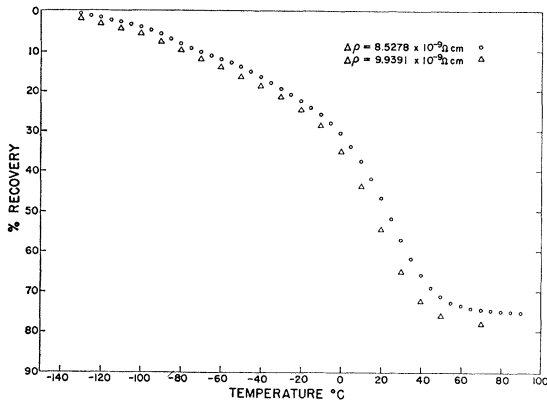


FIG. 8. Isochronal of Au+0.041 Mg, percent recovery versus temperature.

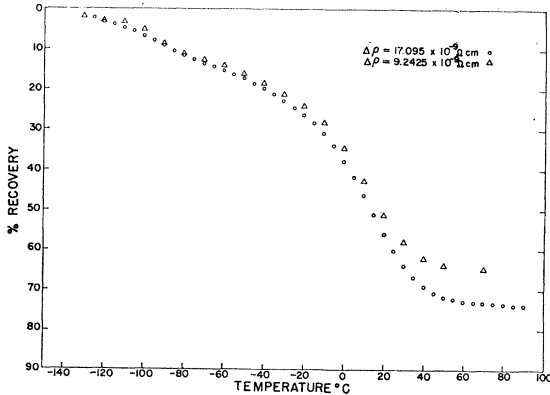


FIG. 9. Isochronals of Au+0.11 Mg, percent recovery versus temperature.

room temperature and so provided a low level of background annealing which can be seen not to have affected the shape of the peak structure appreciably. Note also that above 70°C some samples show appreciable annealing. In the opinion of the author, this results from migration of the solute atoms as has been explained

in the section on preparation of samples. It is then suggested that one should neglect the annealing peaks above 70°C in specimens which had not been annealed before irradiation.

The slopes of the isochronals were determined every 5°C and were plotted versus temperature was dashed

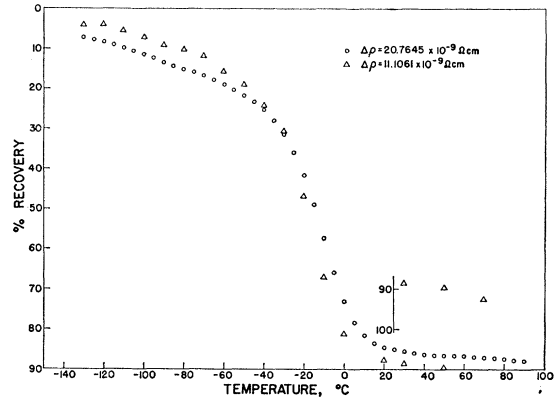


FIG. 10. Isochronals of Au+0.011 Al, percent recovery versus temperature.

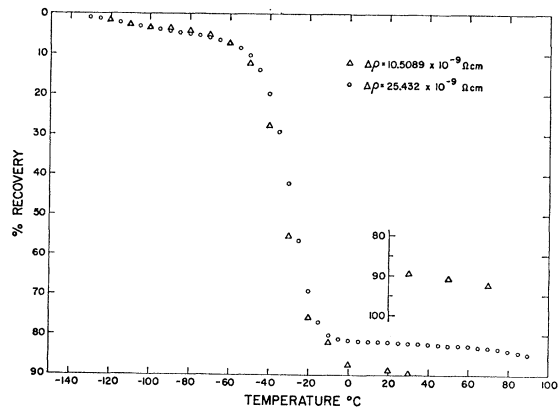


FIG. 11. Isochronals of Au+0.15 Al, percent recovery versus temperature.

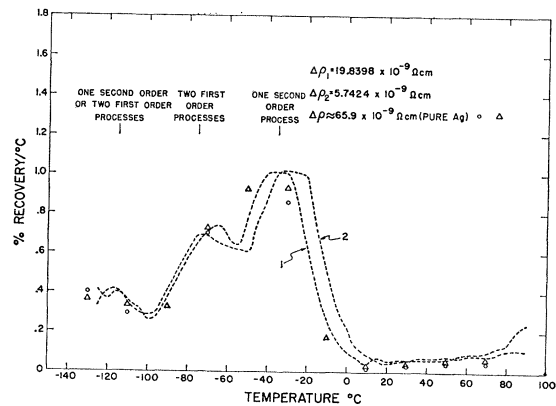


FIG. 12. Slope of isochronal versus temperature for Ag+0.011 Be.

curves in Figs. 12 through 22. This procedure gave excellent resolution of the annealing behavior.

Because of the radical behavior of Ag+0.019 Li, which showed as high as 190% recovery at room temperature, as is shown in Fig. 5, as well as its unreliable resistance ratio behavior described earlier, further investigation of this alloy system was dropped.

D. Determination of the Activation Energy by the Slope-Change Method

To evaluate the migration energy of the defects, the change in slope method was employed as described in Appendix III. This required a series of isothermal annealing curves taken at small temperature intervals,

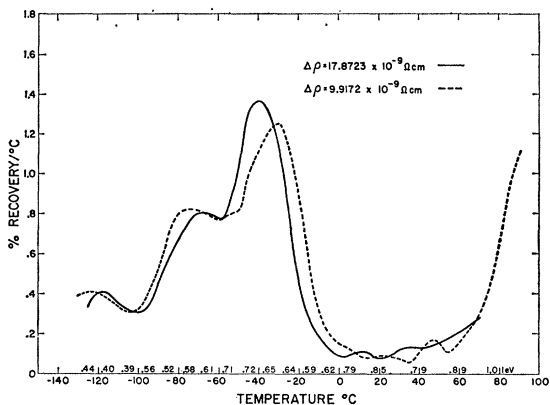


FIG. 13. Slope of isochronal versus temperature for Ag+0.04 Be.

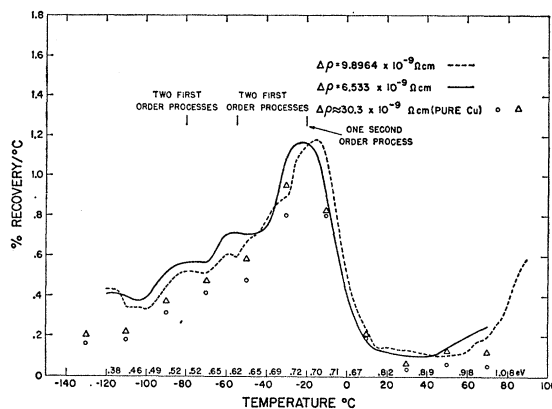


FIG. 16. Slope of isochronal versus temperature for Cu+0.07 Be.

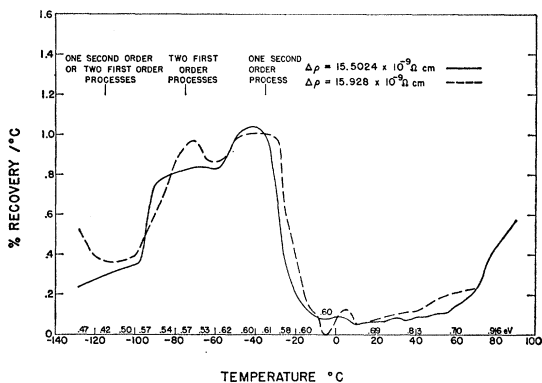


FIG. 14. Slope of isochronal versus temperature for Ag+0.14 Be.

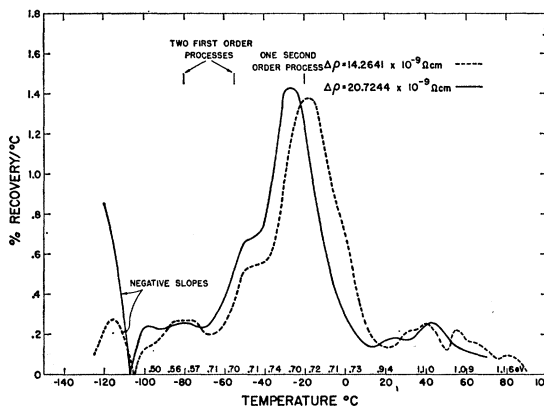


FIG. 17. Slope of isochronal versus temperature for Cu+0.19 Be.

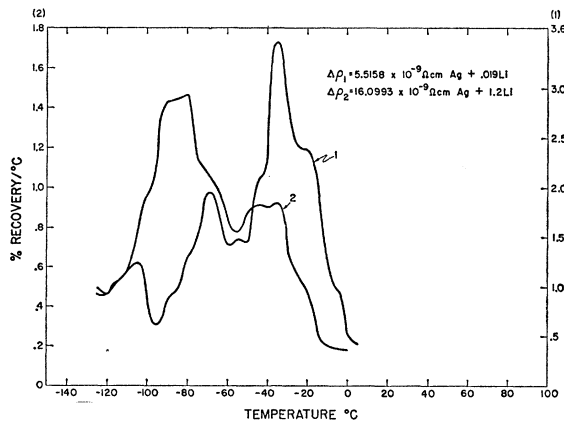


FIG. 15. Slope of isochronal versus temperature for Ag+0.019 Li and Ag+1.2 Li.

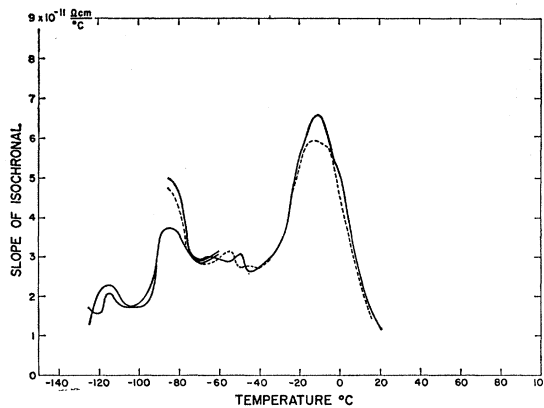


FIG. 18. Slope of isochronal versus temperature for pure Cu as reported by Dworschak, Herschbach, and Koehler (Ref. 13).

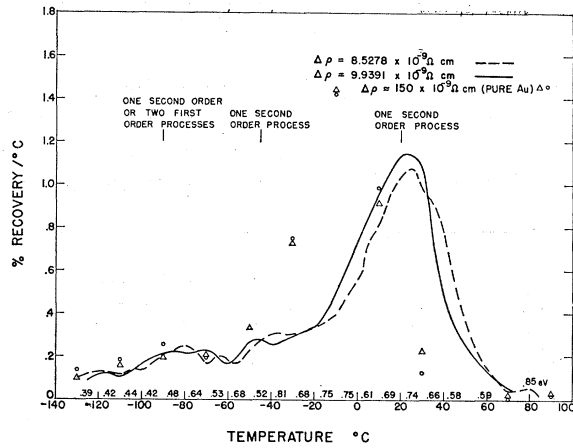


FIG. 19. Slope of isochronal versus temperature for Au+0.041 Mg.

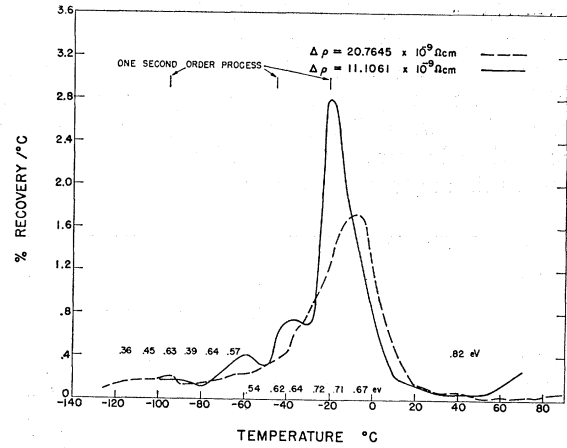


FIG. 21. Slope of isochronal versus temperature for Au+0.011 Al.

since in this method it is assumed that the frequency factor at neighboring isothermal annealing temperatures is equal. It is also assumed that the process occurring is singly activated and that the activation energy is constant between these temperatures. It thus was decided to do 32-min isothermals every 10°C so as to satisfy these assumptions as well as possible and still get enough annealing to maintain accuracy. The residual resistivity of the samples was measured at 2, 4, 8, 16, and 32 min by rapidly removing the sample block from the temperature bath and thrusting it into liquid nitrogen. The block was then placed in liquid helium. The warm-up procedure in the annealing cryostat is discussed earlier. The activation energies determined by this procedure are displayed as parameters in Figs. 12 through 22. Due to a mechanical failure in one of the Au-Al blocks, no activation energies are given between 0 and 40°C for this alloy system. Also note that once the main annealing peaks of the various alloys were passed, isothermals were taken only every 20°C.

From these isothermals, isochronals were obtained where the total time of anneal at each temperature was now 32 min. These isochronals are shown simultaneously with the 10-min isochronals in Figs. 2 through 11. Again the slopes were taken and displayed as a function of the temperature as solid lines in Figs. 12 through 22, showing remarkable similarity to the data taken from the isochronals which were performed every 5°C for 10-min periods. Note that the annealing peaks of the 32-min isochronals are shifted down in temperature. This is due to the longer annealing times at each temperature and not to a dose dependence.

Comparing the activation energies of pure and alloyed material, one notes that in copper there is no change in the activation energy of the stage-III defect, $E_{III}^M = 0.70 \pm 0.04$ eV. In Ag+0.14 Be the activation energy is decreased to about 0.61 ± 0.04 eV, whereas in Ag+0.044 Be the average is about 0.67 ± 0.04 eV as it is in pure silver. In the Au-Mg system both alloys have three separate peaks, as shown in Fig. 25 with an average activation energy of 0.59, 0.68, and 0.75 ± 0.04 eV and in Au-Al both alloys have values of 0.56, 0.65, and 0.72 ± 0.04 eV, which are markedly different from

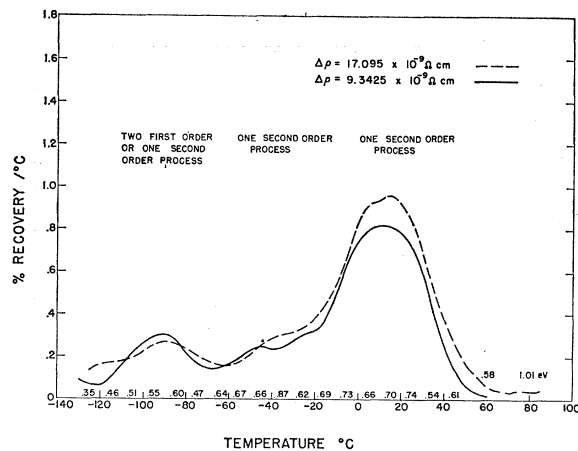


FIG. 20. Slope of isochronal versus temperature for Au+0.11 Mg.

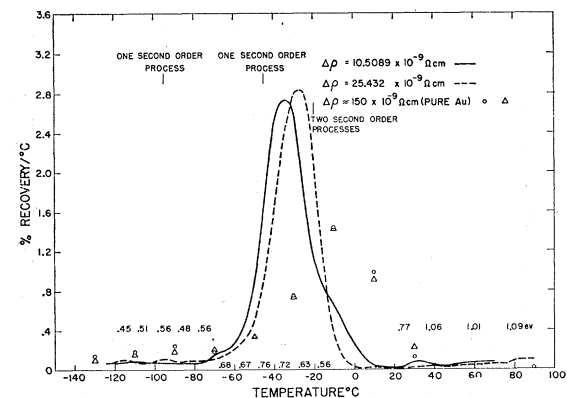


FIG. 22. Slope of isochronal versus temperature for Au+0.15 Al.

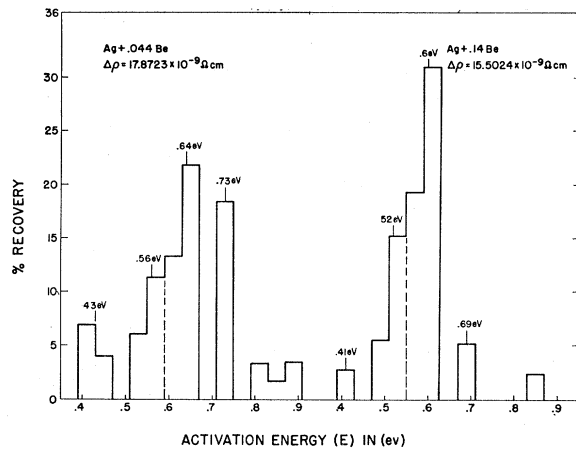


FIG. 23. Percent recovery versus activation energy.

the value in pure gold of 0.80 eV. (All activation energies for pure materials are those given by Dworschak, Herschbach, and Koehler¹³ and by Bauer and Sosin for electron irradiated gold.¹⁶)

To illustrate the structure of the activation energy spectrum, histograms using intervals of 0.04 eV are plotted versus the percent recovery in this interval in Figs. 23 through 26. The average values of the various peaks are shown. These averages simply divide the area under the curves as evenly as possible.

E. Determination of the Order of Kinetics

The order of reaction associated with the various annealing peaks was then determined. Isothermal anneals were taken for four hours at temperatures chosen so as to anneal as near the center of a peak as possible. This isothermal data was then fit to either second-order or first-order kinetics as described by their

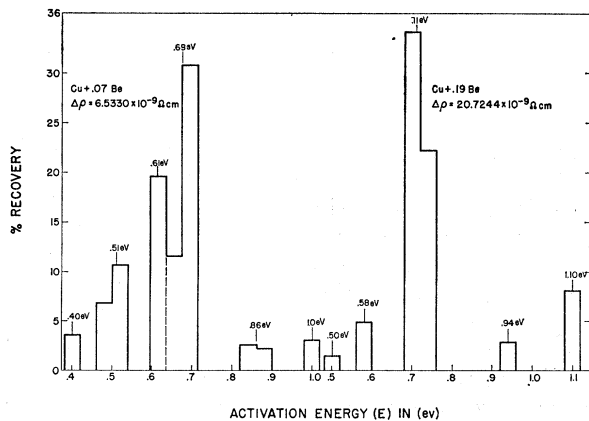


FIG. 24. Percent recovery versus activation energy.

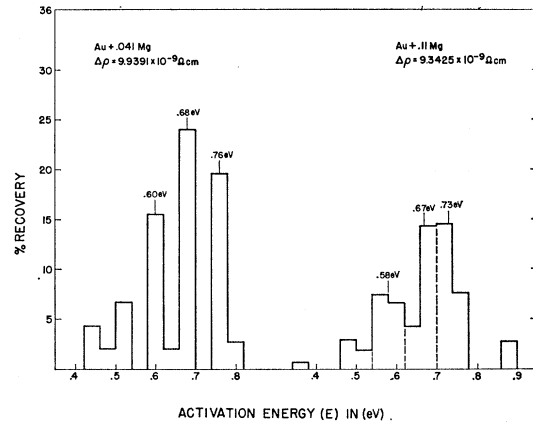


FIG. 25. Percent recovery versus activation energy.

respective kinetic equations, i.e.,

$$(\rho_t - \rho_\infty)^{-1} = (\rho_0 - \rho_\infty)^{-1} + ((\sigma\nu A/\delta)e^{-E/kT})t, \quad (1)$$

$$\ln(\rho_t - \rho_\infty) = \ln(\rho_0 - \rho_\infty) - (\sigma\nu A e^{-E/kT})t. \quad (2)$$

The symbols are as follows: ρ_0 , ρ_t , and ρ_∞ are the resistivities at the beginning of the anneal, at a general time t , and after an infinite time, respectively; σ is the number of atomic sites around a trapped defect within which the migrating defect is certain to be annihilated and will be defined as the capture number; A is the entropy factor, E is the activation energy, k is Boltzmann's constant; T is the absolute temperature; and δ is the resistivity associated with the defects which are annihilated. (The resistivity decrease associated with a decrease in defect concentration of x would be $x\delta$.)

In copper and silver the main peak in stage III was found to obey second-order kinetics as shown in Figs. 27 and 28. The isothermal anneals taken on the annealing peak on the low-temperature side of stage III fit two first-order reactions and will be denoted as stage II, in copper and silver. These results agree with Dworschak, Herschbach, and Koehler's work on pure copper and silver.¹³

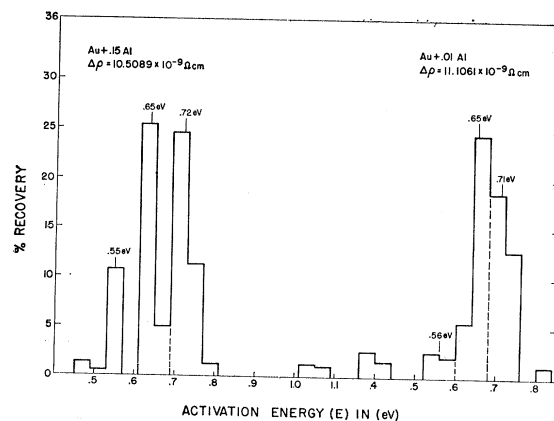


FIG. 26. Percent recovery versus activation energy.

¹⁶ Walter Bauer and A. Sosin, Phys. Rev. 136, A255 (1964).

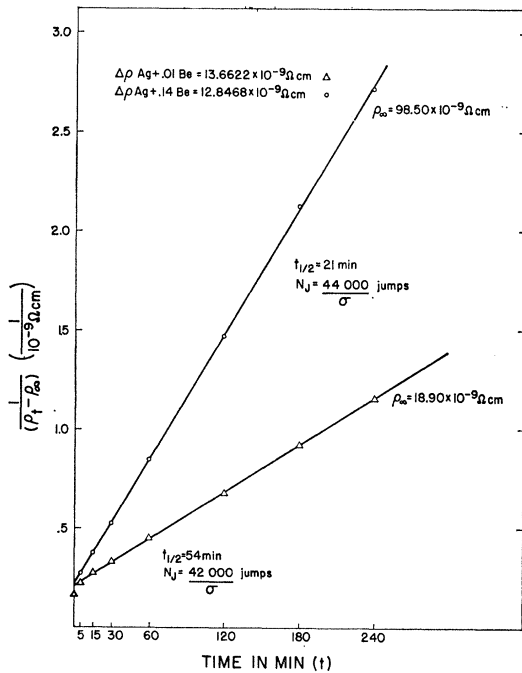


FIG. 27. Fit to second-order process in Ag+0.01 Be and Ag+0.14 Be for anneal at -35°C .

In Au-Mg the isothermal anneal at -90°C fits both one second-order or two first-order reactions equally well. The isothermal at -45°C fits a single second-order

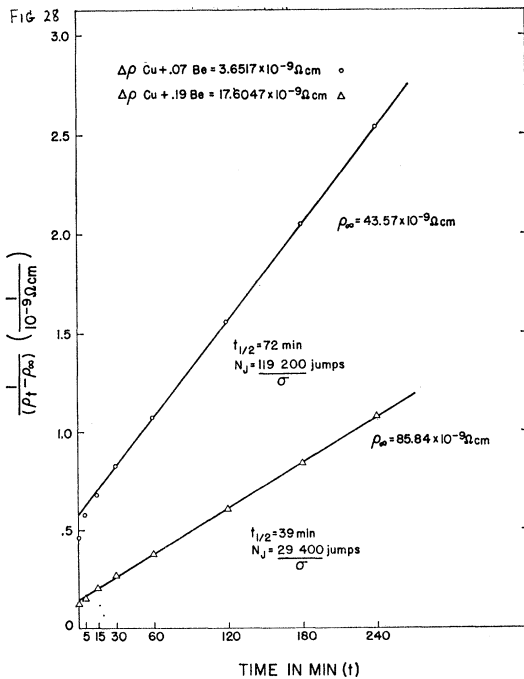


FIG. 28. Fit to second-order processes in Cu+0.07 Be and Cu+0.19 Be for anneal at -20°C .

reaction only, as does the anneal at 20°C on the main peak of stage III as shown in Fig. 29.

In both of the Au-Al alloys the isothermal anneals at -95°C fit one second-order reaction. The isothermal anneals at -45°C indicate that there is most likely one second-order reaction, but it is conceivable that a single first-order reaction is occurring. In Fig. 30 one sees that in Au+0.01 Al the isothermal at -20°C fits one second-order reaction excellently, yet in Au+0.15 Al the isothermal fits two second-order reactions. This can be understood by observing where the annealing peaks are located relative to the isothermal anneals. At -20°C one is just on the edge of the low-temperature side of the main peak in Au+0.01 Al but on the high side of the main peak in Au+0.15 Al. This combined

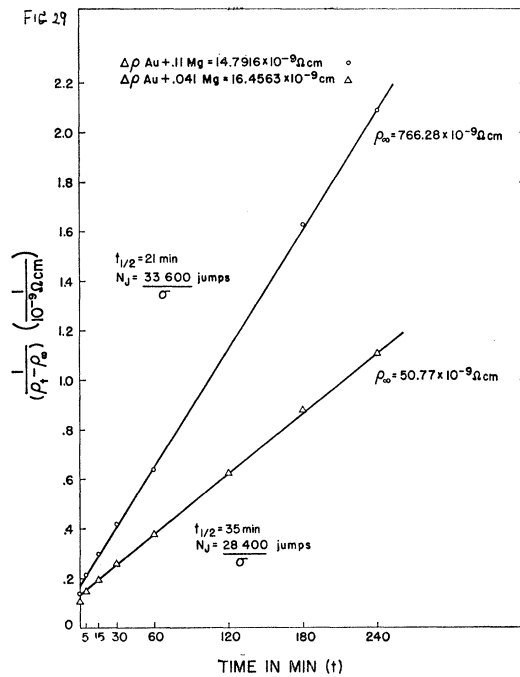


FIG. 29. Fit to second-order process in Au+0.04 Mg and Au+0.11 Mg for anneal at $+20^{\circ}\text{C}$.

with the results above means that the main peak in Au+Al is composed of at least two second-order peaks, one being located on the high-temperature side and one in the center of the peak. Note that Au-Mg shows a second-order peak at -45°C which is separated from the main peak. The main peak has been shifted up in temperature in Au-Mg relative to its position in Au-Al. Also Au-Al obeys second-order kinetics at -45°C besides showing a slight asymmetry on the low-temperature side of the main peak. In Au-Mg the second-order reaction on the high-temperature side of the main peak is not observed because it has probably been swamped by the shift up in temperature of the main peak. It is thus concluded that the gold peak

located in stage III consists of three second-order peaks: a large peak with a small one on each side of it.

F. Determination of the Activation Energy by the Isochronal Method

A second method for obtaining the activation energy of a particular annealing peak was also employed. This method used only isochronal annealing data and the order of reaction. To get a reasonable number of data points using this method, a broad peak with many experimental points was required. This method was thus successfully applied only to the main peaks of the alloys where it has been shown that the kinetics is second order. The equation describing the migration of

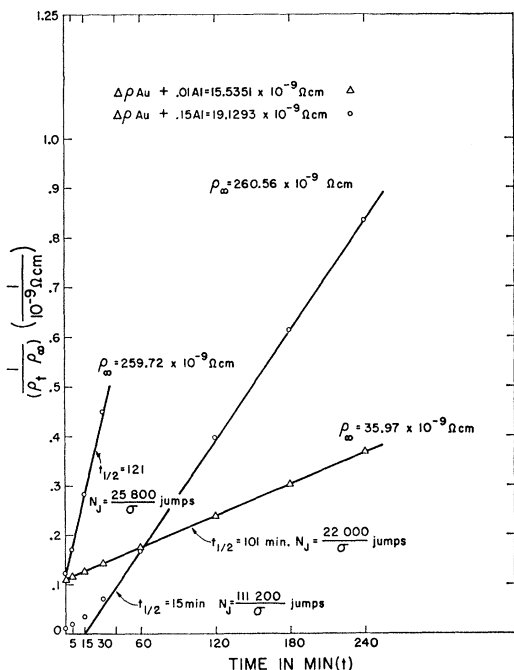


FIG. 30. Fit to one second-order process in Au+0.01 Al. Fit to two second-order processes in Au+0.15 Al for anneal at -20°C .

defects for second-order kinetics in this case is

$$(\rho_f - \rho_{\infty})^{-1} - (\rho_i - \rho_{\infty})^{-1} = ((\sigma\nu A/\delta)e^{-E/kT})(t_f - t_i). \quad (3)$$

In isochronal annealing procedures, $\Delta t = t_f - t_i$ is a constant representing the time spent at each temperature; ρ_{∞} is the resistivity to which the peak is annealing, and so it is a variable parameter in our procedure; ρ_f is the resistivity at the end of each temperature; and ρ_i the resistivity at the beginning of each temperature. Taking the log of this equation yields a straight line where E/k is the slope and $\ln[(\sigma\nu A/\delta)\Delta t]$ the intercept

$$\ln((\Delta\rho_f)^{-1} - (\Delta\rho_i)^{-1}) = \ln((\sigma\nu A/\delta)\Delta t) - (E/k)1/T. \quad (4)$$

Plotting the isochronal resistivity data versus $1/T$ on semilog paper using ρ_{∞} as a variable parameter, a

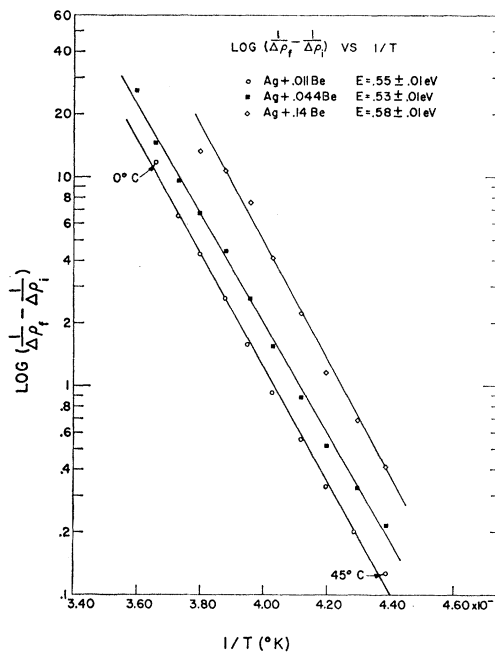


FIG. 31. Plots of isochronal data for Ag+Be alloys in stage III. Second-order annealing is assumed. Slopes give the activation energies shown.

straight line can be obtained. This assumes that both E and $(\sigma\nu A/\delta)$ are constant over the entire fit. These plots for copper and silver are shown in Fig. 31 and

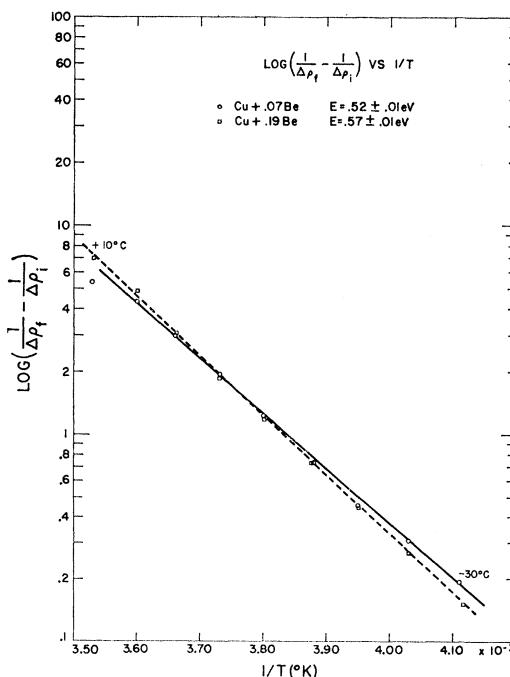


FIG. 32. Plots of isochronal data for Cu+Be alloys in stage III. Second-order annealing is assumed. Slopes give the activation energies shown.

Fig. 32. In the case of the gold alloys a curve which separated into three straight lines was invariably arrived at for all reasonable values of ρ_∞ . This set of three lines was the first indication that there were three separately activated peaks in gold as described above.

The copper data can be fit to a straight line over the entire annealing peak, but gives activation energies of $E=0.52\pm 0.03$ eV for Cu+0.07 Be and 0.57 ± 0.03 eV for Cu+0.19 Be which do not agree with the activation energy determination of $E=0.71\pm 0.04$ eV using the change of slope method by Dworschak, Herschbach, and Koehler¹³ and the present authors.

The activation energies arrived at for Ag+0.011 Be, Ag+0.044 Be, and Ag+0.14 Be, using the isochronal method, are, respectively, 0.55 ± 0.03 eV, 0.53 ± 0.03 eV, and 0.58 ± 0.03 eV, which do not agree with Dworschak, Herschbach, and Koehler's¹³ value of $E=0.67\pm 0.04$ eV. Again a good fit is obtained throughout the entire peak except below -45°C , where because of the overlapping of the first-order peak and the main second-order peak, the bad fit is understandable.

The isochronal method of analysis then yields reproducible results for the activation energies for copper and silver alloys, but these energies are markedly different than those calculated using the change of slope method. Sosin and Rachal¹⁰ calculated an activation energy of 0.45 eV for aluminum and Meechan and Brinkman¹⁷ calculated one of 0.60 eV for copper using this isochronal method. Comparing these values to 0.61 eV¹⁸ for aluminum and 0.71 eV¹³ for copper, as arrived at using the change of slope method, it is observed that others have also found that the isochronal method yields a lower activation energy than does the change in slope method.

Let us investigate possible reasons for this disagreement. The isochronal method assumes that the activation energy E , as well as the frequency factor $\sigma\nu A$, is constant throughout the entire peak. From the change of slope method a spread of activation energies is observed as the histograms illustrate, even though from the isothermal studies the main peaks seem to be singly activated. Also note that the "straight lines" in Figs. 31 and 32 actually have a continuous wiggle, indicating that rather than having a single activation energy the peak might be multiply activated. This then suggests that it might be too great a restriction to say that the peak has a single activation energy over the entire range. It is most likely that there is such a wide spread in energy about the main activation energy that the assumption used in analyzing the isochronal data is too restrictive in the case of stage III for copper and silver.

The amount of damage that anneals in each peak is compared in Table IV. The percent of recovery in each

peak is calculated by using the amount of damage which anneals out from -130°C to the end of the main stage-III peak as 100% recovery. The temperatures chosen to delineate a peak are given. The consistency between the percents annealing in each peak is remarkable.

V. DISCUSSION OF RESULTS

A. Existing Models

The most startling feature of the present data on alloys is their strong similarity to the data for pure silver and copper¹³ as compared in Figs. 12, 16, 18, 19, and 21. Because the gold alloys acts differently from pure gold, it will be discussed separately.

From Table III it is observed that as the amount of solute is increased in silver and copper the production rate increases. This indicates that stage-I interstitials migrate and are stopped at the impurity sites before they have a chance to annihilate. It will be assumed that interstitials are the mobile defect in stage I in copper and silver.¹⁻⁵ A large portion of the damage which normally anneals out in stage I is thus present in the alloyed samples after irradiation at 80°K . Three models to explain stage III will be discussed: (1) the interstitial vacancy (i-v) model, (2) the two-interstitial model, and (3) the interstitial di-interstitial model.

B. The Interstitial-Vacancy Model in Stage III

Consider first the interstitial vacancy model. In this model interstitials migrate in stage I and vacancies in stage III. In pure copper and silver the interstitials present in stage III are trapped in clusters, but in the alloys used here some interstitials are also trapped by impurities, as will be discussed below. The vacancies migrating in stage III in pure copper and silver thus annihilate at interstitials present in clusters, while those migrating in alloys annihilate at interstitials trapped in clusters and at impurities. The rate of recovery would, of course, obey second-order annealing kinetics for a random walk of vacancies to interstitials since the number of jumps to annihilation would be inversely proportional to the total damage present.

Furthermore, in this model it is reasonable to suppose that no free vacancies are left after stage III, as is observed in the case of pure silver where Herschbach, Dworschak, and Koehler¹³ found no evidence for vacancy migration at temperatures above stage III and below 80°C , i.e., below 0.88 eV. Remember that vacancies in silver migrate with energy 0.83 eV.

C. The Interstitial-Vacancy Model in Stage II

The above model fits only the region obeying second-order kinetics in stage III, since this model would require a random walk of vacancies to interstitials. Consider the first-order peaks located on the low-temperature side of the main peak in copper and silver.

¹⁷ C. J. Meechan and J. A. Brinkman, Phys. Rev. **103**, 1193 (1956).

¹⁸ S. Ceresara, H. Elkholy, and T. Federighi, Phys. Rev. Letters **16**, 8 (1965).

TABLE IV. The fraction of damage that anneals in each recovery peak for various alloys.

Material	Peaks from T_1 to T_2 (°C)	Fraction recovering early in stage II (%)	Peaks from T_1' to T_2' (°C)	Fraction recovering late in stage II (%)	Peaks from T_1'' to T_2'' (°C)	Fraction recovering in stage III (%)	Fraction of recovery through stage III (%)
Ag+0.01 Be	-130 to -100	14.1	-100 to -55	32.6	-55 to 20	52.5	74.5
Ag+0.01 Be	-130 to -100	13.0	-100 to -50	35.4	-50 to 10	51.5	80.0
Ag+0.044 Be	-130 to -100	11.5	-100 to -60	34.5	-60 to 15	54.0	87.0
Ag+0.044 Be	-130 to -105	11.2	-100 to -60	34.2	-60 to 0	54.6	80.5
Ag+0.14 Be	-130 to -100	14.8	-100 to -60	37.6	-60 to -5	47.5	81.0
Ag+0.14 Be	-130 to -100	8.4	-100 to -60	42.0	-60 to -5	49.6	71.5
Cu+0.07 Be	-100 to -70	21.6	-70 to -45	13.1	-45 to 20	65.5	65.0
Cu+0.07 Be	-100 to -75	19.1	-75 to -55	13.2	-55 to 15	67.6	68.0
Cu+0.19 Be	-105 to -70	10.9	-70 to -40	17.2	-40 to 20	72.0	64.0
Cu+0.19 Be	-110 to -75	10.0	-75 to -45	19.9	-45 to 10	77.0	63.0
Au+0.041 Mg	-100 to -55	12.3	-60 to -15	12.3	-15 to 70	69.2	73.0
Au+0.11 Mg	-110 to -60	12.5	-60 to -20	11.8	-20 to 70	69.8	76.0
Au+0.11 Mg	-105 to -60	14.2	-60 to -30	10.6	-30 to 70	71.0	71.5
Au+0.11 Mg	-120 to -70	15.9	-70 to -30	12.7	-30 to 70	70.0	63.0
Au+0.01 Al	-130 to -80	10.2	-80 to -30	21.0	-30 to 30	68.8	78.5
Au+0.01 Al	-130 to -80	7.8	-80 to -30	24.2	-30 to 30	68.0	84.5
Au+0.15 Al	-130 to -75	5.5			-75 to 0	94.5	80.5
Au+0.15 Al	-130 to -80	4.0			-80 to 15	96.0	88.0

These peaks will be designated as stage II. Because stage II is first order, only certain mechanisms for annihilation are possible. It is possible that either vacancies or interstitials migrate to dislocations, grain boundaries, or impurities or that correlated interstitial-vacancy annihilation occurs. The first two possibilities are extremely remote because of the large grains and low density of dislocations in annealed samples. Also the annealed pure copper and unannealed Cu+0.07 Be have very similar peak structure indicating a weak or negligible dislocation affect. The possibility of migration to impurities was ruled out by Dworschak and Koehler¹⁹ who noted that by increasing the damage by a factor of 10 in pure copper no alteration of stage II was observed, indicating that stage II was an intrinsic and not impurity-dependent recovery stage.

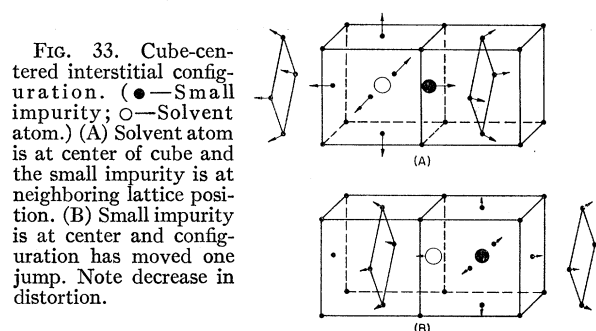
Consider then the possibility of correlated close pair i-v annihilation by vacancy migration. Suppose that some interstitials are trapped in clusters and some by impurities in the alloys so that they are not eliminated in stage I even though a correlative force exists. Some of these correlated pairs would then remain intact up to stage II where vacancies would begin to migrate yielding correlated close-pair interstitial-vacancy recombination by vacancy migration. This would, of course, require deep trapping of the interstitial.

Judging from the data, the ability of the impurities to create close pairs seems to rise sharply near 0.1 at.% and above. This would seem reasonable since this would be one impurity per 1000 base atoms or about one impurity every ten lattice spacings in any direction. This is born out by the Ag-Li data. In the case of Ag+1.2 Li, any defect is less than seven atomic

distances from an impurity, whereas in Ag+0.019 Li a defect is less than 25 atomic distances from an impurity and Ag+1.2 Li shows a marked impurity affect in stage II whereas Ag+0.019 Li shows only a mild one.

D. The Impurity-Trapping Mechanism

Consider the mechanism for the trapping of interstitials by impurities. Figure 33 shows a cube-centered interstitial in an fcc lattice. Since the lattice is close packed and since the central copper or silver atom, as the case may be, has a reasonably large closed shell the nearby lattice atoms are displaced outward as shown. Suppose the interstitial migrates by an interstitialcy mechanism, moving towards the right. This displaces the beryllium atom into the center of the next cube. The copper or silver atom which was originally in a cube-centered position is now in a lattice position and the beryllium which was in a substitutional position is now in a cube-centered interstitial position. Since the beryllium ion core is small relative to that of copper or



¹⁹ F. Dworschak and J. S. Koehler, Phys. Rev. **140**, A941 (1965).

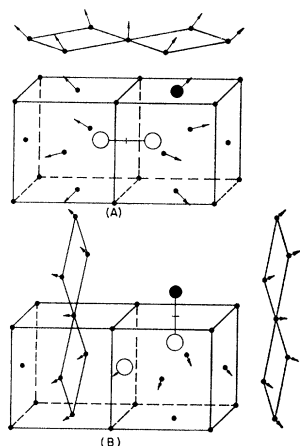


FIG. 34. Split interstitial configuration. (●—Small impurity; ○—solvent atom.) (A) Solvent atoms are in split interstitial configuration and the small impurity is at a neighboring lattice position. (B) Small impurity is in split interstitial configuration with solvent atom after interstitial has jumped once. Note decrease in distortion.

silver, the outward displacements will be smaller with beryllium in the cube-centered position than with copper or silver in the cube-centered position. Huntington²⁰ showed that about 84% of the total energy of formation of the interstitial is associated with closed-shell repulsion, the remainder arising from charge interactions. Moreover, the total formation energy is large, being of the order of 4 eV. It is quite possible then that large trapping energies can occur. Note that the closed-shell volume of beryllium is 1/56 that of silver and 1/27 that of copper, thus leading to a smaller dilatation of the base atoms about a beryllium interstitial.

Even if the equilibrium interstitial configuration is the split (100) configuration, as shown in Fig. 34, a similar trapping will occur although the magnitude of the binding energy between the interstitial and the impurity would probably be smaller than in the case of the cube-centered interstitial since the lattice distortion is largely determined by the nature of the two atoms which define the axis of the defect.

For the impurities used in the present experiment, the trapping is sufficiently strong that interstitials are not released during annealing at temperatures below stage III. Some investigators have observed new annealing peaks below stage III in their alloy experiments. Blewitt and co-workers⁹ found that Cu+0.1 Si shows a large amount of recovery at 150°K, while in pure copper and Cu+0.1 Be recovery is observed at about 230°K. Similarly Sosin and Rachal¹⁰ found an annealing stage at 150°K in Al+0.1 Zn whereas stage III occurs at about 220°K in pure aluminum.

E. The Number of Jumps to Annihilation and the Frequency Factors in Stages II and III

Since close-pair recombination is characterized by one or two jumps to annihilation, it would be of interest to investigate the number of jumps experimentally. The number of jumps to annihilation N_J , can be

expressed as follows:

$$N_J = (\nu A e^{-E/kT}) t_{1/2}. \quad (5)$$

Here ν is the frequency factor, A the entropy factor, T the absolute temperature, E the activation energy, k Boltzmann's constant, and $t_{1/2}$ the time for the resistivity to halve during [a particular isothermal anneal. For first-order plots the slope is $c_s \nu A e^{-E/kT}$, c_s is the sink density which is one for close pair recombination, $t_{1/2}$ is $\ln 2$ divided by the slope. If E is known, taking $\nu A = 10^{12} \text{ sec}^{-1}$, experimental annealing rates enable us to check this c_s . In Ag+0.01 Be and Ag+0.14 Be, with initial damages at 80°K of $\Delta\rho = 13.66 \times 10^{-9} \Omega \text{ cm}$ and $\Delta\rho = 12.85 \times 10^{-9} \Omega \text{ cm}$, the number of jumps to annihilation at -75°K is 1.5 and 16 jumps, respectively, for stage II. In Cu+0.07 Be and Cu+0.19 Be with damage at 80°K of $\Delta\rho = 3.55 \times 10^{-9} \Omega \text{ cm}$ and $\Delta\rho = 17.60 \times 10^{-9} \Omega \text{ cm}$, the number of jumps at -55°K is 2.5 and 27 jumps, respectively, for stage II. This indicates that only one or two jumps are required to achieve interstitial vacancy recombination in copper and silver in stage II, and, therefore, stage II probably corresponds to correlated close pair recombination. Also note that in Cu-Be a change in the amount of damage by a factor of five does not alter the number of jumps. This also indicates that stage II obeys first-order annealing kinetics since the number of jumps in a first-order annealing process should show no dependence on the concentration of defects as is observed.

From Eq. (1) it can be seen that a slightly modified frequency factor can be expressed in terms of experimental observables, with a minimum of assumptions, for stage III, as

$$\sigma \nu A = (\delta / \Delta\rho_0) (e^{E/kT} / t_{1/2}). \quad (6)$$

From the slope-change method discussed earlier, the activation energies are known. $1/\Delta\rho_0$, and half-life $t_{1/2}$ can be determined from our isothermal fits to second-order kinetics. Remember that δ is the resistivity change associated with the annihilation of stage III defects. Assuming that the resistivity decrease in stage III is due to interstitial vacancy recombination then a reasonable value for δ is $2 \times 10^{-4} \Omega \text{ cm}$. The modified frequency factor $\sigma \nu A$ can thus be determined. In the Ag-Be and Cu-Be systems, the activation energies will be taken as $E_{\text{III}}^m = 0.65 \pm 0.04$ and 0.71 ± 0.04 eV, respectively. The frequency factors thus calculated for Ag+0.01 Be, Ag+0.14 Be, Cu+0.07 Be, and Cu+0.19 Be are $0.76 \times 10^{15 \pm 0.8}$, $2 \times 10^{15 \pm 0.8}$, $3.9 \times 10^{15 \pm 0.8}$, and $1.8 \times 10^{15 \pm 0.8}$ cps, respectively.

Using Dworschak and Koehler's¹⁹ data for a 1700-min isothermal performed on copper at 263°K, the frequency factor can be calculated to be $1.7 \times 10^{15 \pm 0.8}$ cps. In order to obtain the frequency factor for pure silver, two isothermals reported by Dworschak, Herschbach, and Koehler,¹⁸ one at -30°K and one at -10°K, were normalized to a single isothermal at -10°K by the use

²⁰ H. B. Huntington, Phys. Rev. 91, 1092 (1953).

of the time-correction method described in Appendix I. The two isothermals were combined in order to get the longest possible isothermal so as to have the best fit possible and, therefore, the best slope determination. This longer isothermal was then fit to second-order kinetics. Using the slope of this plot, the assumed value for δ of 2×10^{-4} Ω cm, and the activation energy which they reported to be $E = 0.67 \pm 0.04$ eV, the frequency factor is calculated to be $\sigma\nu A = 1.2 \times 10^{15 \pm 0.8}$ cps. It is apparent then that the frequency factors in pure copper and silver are unaltered by alloying with beryllium.

In the case of copper and silver, one thus finds that the stage-III annealing process is completely unaltered by alloying. Within the accuracy of the present measurements neither the activation energy, the frequency factor, nor the order of reaction is changed by alloying with small core impurity atoms chosen to trap interstitials. Such a situation seems very remarkable if some kind of an interstitial is supposed to migrate in stage III in copper and silver. The only change which occurs upon alloying is an increase in the fraction of the damage which recovers in stage III. This increase is associated with a decrease in the stage-I annealing.

F. Difficulties with the Interstitial-Vacancy Model

Although the interstitial vacancy model fits the experimental results with a minimum of assumptions, there is one discrepancy between the results predicted by the model and the observed phenomena. A major difficulty with the model is that the energies of migration of vacancies, as obtained both in quenching and equilibrium experiments, are generally about 10 to 15% larger than the migration energies associated with stage-III annealing, as determined by radiation-damage experiments. This comparison is made in Table V.

Although the above difficulty is encountered, it is reasonable to expect that stage III is associated with vacancy migration since of the two defects produced by irradiation one, the interstitial, has already moved in stage I leaving the vacancy. Moreover, the stage-III energy is almost the vacancy migration energy. The model, therefore, provides a natural explanation for why the stage-I and stage-III migration energies differ. It also provides an easy explanation of the lack of influence of small-core impurities on stage III.

The fact that an appreciable amount of damage remains after stage III in a proton irradiated specimen can only be understood, using the interstitial vacancy picture, if it is supposed that the vacancies which migrate in stage III can be immobilized in some way, perhaps in clusters. From Dworschak and Koehler's¹⁹ work the annealing which occurs in a pulsed sample of proton irradiated copper does not show evidence of anything other than stage-III annealing even though specimens were heated to about 230°C. Moreover, the

TABLE V. Activation energy E_{III} of the stage-III defect, and vacancy migration energy E_V , in various elements.

Material and lattice	E_{III} (eV)	E_V (eV)	E_{III}/E_V^a
Al fcc	0.61	0.65	0.94
Ni fcc	1.03	1	1.03
Cu fcc	0.71	0.88	0.81
Ag fcc	0.67	0.83	0.81
Pt fcc	1.20	1.38	0.87
Au fcc	0.80	0.83	0.96
Fe bcc	0.9		
Nb bcc	1.3		
Mo bcc	1.23		
W bcc	1.7	2.02	0.84
Average ^a			0.89 \pm 0.07

^a Note that in both E_V and E_{III} there is an uncertainty of about 0.04 eV so that by adding the uncertainties in taking the above ratio, one sees that the spread in E_{III}/E_V lies within the experimental error.

damage remaining in the pulsed specimens was at least as large as that remaining in the copper samples annealed at room temperature. (See Fig. 3 and Fig. 4 of Dworschak and Koehler.¹⁹)

G. The Two-Interstitial Model in Stages II and III

The two-interstitial model will now be investigated in relation to the present experiment. In this model there is a metastable interstitial moving in stage I, with an activation energy of about 0.10 eV, and a stable, less mobile defect which migrates in stage III, with an activation energy of about 0.70 eV. Originally, it was proposed that the metastable interstitial be the crowdion which was supposed to migrate along its axis in stage I, but the fact that stage I obeys second-order kinetics not third order as one would expect for one-dimensional motion makes this proposal rather unattractive.³ A further trouble with this proposal is the difficulty encountered in devising concrete models for the two interstitials. Each interstitial must be able to migrate in three dimensions, the metastable interstitial must be able to convert into the stable interstitial,¹⁹ and these requirements must be met both in the fcc and bcc crystals. The proponents of this model have not yet given detailed models for the two interstitials in a bcc lattice nor have they described how atoms rearrange during conversion in either the bcc or fcc case.

In pure copper and silver both the stable and metastable forms of the interstitial would have to be produced during irradiation, but in heavy-particle irradiation, a larger fraction of stable interstitials is produced than in electron irradiation. This would be necessary since stage III accounts for a larger fraction of the annealing in heavy-particle irradiation than in electron irradiation of copper and silver. If the irradiation is done at 80°K, the metastable interstitial migrates at this irradiation temperature. Some of the metastable interstitials are annihilated while others are stopped at impurities. Suppose then that the impurities are capable

of both converting some of the metastable interstitials into stable interstitials without trapping and trapping some of the interstitials without conversion. This then would lead to an increase in the rate of production at 80°K as is observed. The trapped metastable interstitials would be released at higher temperatures depending on the binding energy B of the trap. This would introduce some new annealing peaks in stage II, as observed by some investigators.^{9,10} The converted interstitials would then proceed to anneal in stages II and III as if there were no impurity present as long as these stable interstitials were not also trapped, and the stage-III interstitials would obey second-order annealing kinetics as in pure silver and copper. Because no new peaks were observed in the present work, it is apparent that the solute atoms used in this experiment in copper and silver must only convert the metastable defects. The two-interstitial model thus is in agreement with the data for copper and silver alloys for the second-order part of stage III, as long as certain assumptions are made.

Consider next the two-interstitial model in relation to stage II which obeys first-order kinetics. It is required as it was in the interstitial-vacancy model that there be close-pair correlated interstitial-vacancy annihilation with the stable interstitial migrating only a few jumps in stage II. The arguments for vacancy migration in stage II made above follows similarly for the interstitial model. The slight alteration is that the impurities would now have to convert the recoiling atom into the stable form of the interstitial before it moves more than a few lattice sites from its original position.

H. Difficulties with the Two-Interstitial Model

The objections to the two-interstitial model are (1) the inability of its proponents to create two models of the interstitial with the markedly different migration energies of 0.10 and 0.70 eV, (2) the lack of a concrete model governing the conversion of the metastable to the stable interstitial, and (3) the difficulty in understanding why both bcc and fcc metals act so similarly although the geometrical configuration of their interstitials would be expected to differ. One also could ask why an impurity would trap a metastable interstitial in certain instances and convert it in others, and if it converted this interstitial, why it would not also trap the converted defect. This data indicates that, if anything, the activation energy of stage III is slightly reduced, and therefore that the converted defects are not trapped with a detectable binding energy.

One can answer to some degree the question of why some defects might be converted and some trapped by assuming that there is a dependence on the direction from which the metastable defect approaches the impurity atom. Eshelby²¹ found that the strains near a

defect are highly anisotropic and lead to repulsion in some directions and attraction in others. The assumption is thus made more plausible if a repulsion leads to conversion to the stable interstitial and attraction leads to trapping of the metastable form.

I. The Di-Interstitial Model

The di-interstitial model states that a single interstitial runs in stage I whereas a di-interstitial runs in stage III. This model would seem to be discredited by the present experiments on copper and silver alloys. Since the stage-I interstitial is stopped at the solute atoms, it would seem apparent that few dimers could be formed because the number of traps exceeds the number of interstitials by at least a factor of two in all of the present alloys and in some cases by a factor of ten. It would thus be improbable that one could accumulate at each trap two interstitials in order to form a dimer. Although some dimers could be formed, one would expect the number of dimers to be reduced as the impurity level is increased because of the increased number of traps present. The reduction in the percentage of dimers would thus cause stage III to be decreased markedly in the alloys in comparison to stage III in pure silver and copper, but just the opposite effect is observed. Stage III is observed to be increased in magnitude, because of trapping, as the impurity concentration increases, but unchanged in shape, so that the interstitial di-interstitial model seems not to be in agreement with the presently available data.

J. The Production of Damage

The damage rates observed by the present experiments are exceedingly high, even in view of the fact that there is an uncertainty of $\pm 50\%$ in the damage rates reported in Table III. To demonstrate how large these rates are, consider the values of the initial slopes of the production curves observed by Cooper, Koehler, and Marx²² for pure copper, silver, and gold. They used 12-MeV deuterons at 12°K and found production rates for copper, silver, and gold of 2.27, 2.68, and 3.88×10^{-9} $\Omega \text{ cm}/(10^{15} \text{ d}) \text{ cm}^2$, respectively.

Now a simple theory of displacement, as given by Seitz and Koehler,²³ yields Eq. (7):

$$dN/d\Phi = \sigma_a \bar{\nu} n_0, \quad (7)$$

where N is the number of displaced atoms per unit volume, Φ is the integrated flux, σ_a is the primary displacement cross section, $\bar{\nu}$ is the average number of displacements per primary displaced atom, and n_0 is the number of atoms per unit volume of the irradiated material. Now $\bar{\nu}$ depends only logarithmically on the

²² H. G. Cooper, J. S. Koehler, and J. W. Marx, *Phys. Rev.* **97**, 599 (1955).

²³ F. Seitz and J. S. Koehler, in *Solid State Physics*, edited by F. Seitz and D. Turnbull (Academic Press Inc., New York, 1957), Vol. 2, p. 406.

²¹ J. D. Eshelby, *Acta Met.* **3**, 487 (1955).

mass and energy of the incident particle. Moreover, the energies of the protons and deuterons used were not very different. The cross section σ_a is proportional to the mass of the incident particle, therefore, the deuteron results should be divided by two in order to make a comparison with the proton results obtained on dilute alloys. Hence, comparing Cooper, Koehler, and Marx's²² results with present results listed in Table III, it is seen that irradiation of alloys at 80°K gives considerably larger damage production rates than those seen in pure metals at 12°K. This difference is particularly noticeable in Au-Al where the production in the alloy is more than three times that in pure gold. Note that the effect is observed in all three of the noble metals. It would be valuable to have a comparison of the damage rate at 10°K in electron irradiated pure noble metals and alloys. Sosin and Neely²⁴ have done such experiments on Cu-Be alloys, but unfortunately they do not give production rates.

The large alloy production rate in silver and copper can be explained using the interstitial-vacancy model if one supposes that some interstitial migration occurs in the thermal spike during the production of a damaged region. In the alloys some of the migrating interstitials would then be trapped during the thermal spike, before they could migrate. This interpretation would thus predict that the enhancement in the rate of production would not be as large in electron as in deuteron or proton-irradiation experiments. The reason for this is that in electron irradiation, the thermal spikes are much smaller so that relatively little damage is removed by thermal spikes during electron irradiation. The alloying would also prevent some recovery of damage due to thermal spikes during production if the two-interstitial model were correct since conversion of a metastable interstitial to a stable interstitial is enhanced near an impurity so that the effective production rate would be larger in an alloy than in the pure material.

The fact that only 0.011 at.% of aluminum can increase the production rate by a factor of 3 in pure gold suggests then that some type of defect travels an appreciable distance during production. This could be the focused replacement collisions since the ion-core radius in gold is nearly equal to the atomic radius. If one assumes a capture cross section of ten atoms associated with impurity trapping of focusons and keeps in mind that 0.011 at.% aluminum is trapping these focusons, which propagate in one direction, then a large fraction of these focusons travel about a thousand atomic distances or more. Note that this implies that the reason for the large production rate in gold differs from that in the copper and silver alloys, where interstitial migration during the thermal spike is suggested as the reason the defect reaches the impurities. In the future it would be valuable to do electron irradiation of noble metal alloys. If the above suggestion is correct, little

enhancement in the production rate would be found in copper and silver alloys because thermal spikes are small in electron irradiation, but enhancement would still occur in a gold alloy because the thermal spike in the focuson model is not relevant to the enhancement.

K. The Interstitial Model in Gold

The Venables-Balluffi experiment^{25,26} constitutes strong evidence that interstitial migration occurs in stage III in gold. Venables and Balluffi irradiated gold containing vacancy tetrahedra with 200-eV argon ions at about 170°K and examined the specimen at various temperatures with an electron microscope. Damage clusters were observed near the bombarded surface and tetrahedra in that portion of the specimen were eliminated. Tetrahedra which existed at greater distance than 300 Å into the specimen from the bombarded surface were unaltered. The specimen was then gradually warmed. At about -10°C the tetrahedra were observed to shrink. Since this is approximately the temperature appropriate for stage III, it is supposed that at -10°C interstitials resulting from ion bombardment become mobile in gold. They migrate to tetrahedra and are annihilated there, causing shrinkage.

The present alloy experiments show that stage III in alloyed gold shows three second-order processes whose activation energies and frequency factors are compared with those of pure gold in Table VI. The frequency factor for pure gold is calculated using Dworschak, Herschbach, and Koehler's¹³ 64-min isothermals performed at -10 and 10°C. The method used is explained earlier in the section on frequency factors. Note that in the case of gold both the frequency factors and the activation energy associated with stage III suffer appreciable changes on alloying.

Let us speculate about the atomic behavior responsible for these results in gold. Because of Venables and Balluffi's findings and the marked affect of alloying on the annealing behavior, it is felt by the present authors that the stage-III defect in gold is the interstitial. It will further be assumed that the interstitial in gold is

TABLE VI. Activation energies and frequency factors of gold alloys and of pure gold. The designations III_a, III_b, and III_c refer to the small low-temperature annealing peak, the main annealing peak, and the small high-temperature annealing peak, respectively.

Material	Frequency factor ($\sigma v A$) in 10 ¹⁴ cps			Activation energy (E) in eV ± 0.04 eV		
	III _a	III _b	III _c	III _a	III _b	III _c
Au+0.04 Mg	260	1.25	...	0.68	0.76	0.60
Au+0.11 Mg	260	1.0	...	0.67	0.73	0.58
Au+0.01 Al	11.7	0.65	0.71	0.56
Au+0.15 Al	...	101	0.114	0.65	0.72	0.55
Au		12			0.80	

²⁴ A. Sosin and H. H. Neely, Phys. Rev. **127**, 1465 (1962).

²⁵ J. A. Venables and R. W. Balluffi, Phil. Mag. **11**, 1021 (1965).
²⁶ J. A. Venables and R. W. Balluffi, Phil. Mag. **11**, 1039 (1965).

the split (100) interstitial and that it migrates with an activation energy 0.8 eV. What then happens to the interstitial in the alloys? It is possible that the small core impurities occupy the center of the interstitial configuration in the alloys and migrate as interstitials, but not by an interstitialcy mechanism, during stage-III annealing. Since the core of the impurity is smaller than the core of gold and the impurity is now the migrating defect, one can understand why the activation energy might decrease in the gold alloys relative to the pure gold. This suggests that experiments using a larger core impurity would be valuable since the stage-III activation energy should increase as the core size increases.

If stage III in gold is assigned to vacancy migration, then it is difficult to understand why small core impurities influence stage III in gold. It would also be difficult to understand the Venables and Balluffi work. Remember also that no precipitous stage I has yet been observed in gold as in copper and silver. The ion core in gold fills almost the entire lattice whereas it occupies much less of the available volume in copper and silver. Therefore, taking all of the presently available data in hand, it is not too improbable that the stage-III defect in gold is an interstitial and a vacancy in copper and silver.

VI. SUMMARY AND CONCLUSIONS

The main experimental conclusions that can be made regarding the data are as follows: (1) The production rate for irradiation by 12-MeV protons, at 80°K, of dilute alloys of copper, silver, and gold is enhanced in comparison to pure copper, silver, and gold as illustrated in Table III. (2) The shape of the recovery spectrum of Cu-Be and Ag-Be throughout the temperature range of -130 to 90°C is almost identical, as shown in Figs. 12, 16, and 18, to that of pure copper and silver. (3) The activation energies of the stage-III defect in pure copper and silver being 0.71 and 0.67 eV, respectively,¹⁸ remain essentially the same in the alloys. (4) Stage III in Cu-Be and Ag-Be, as in pure copper and silver, is a singly activated second-order recovery stage, whereas stage II is composed of several first-order reactions. (5) The shape of the recovery spectrum of Au-Mg and Au-Al differs from pure gold, as compared in Figs. 19 and 21. (6) Stage III in the gold alloys is composed of three second-order recovery peaks whose activation energies are 0.59 ± 0.04 , 0.68 ± 0.04 , and 0.75 ± 0.04 eV in Au-Mg, and 0.56 ± 0.04 , 0.65 ± 0.04 , and 0.72 ± 0.04 eV in Au-Al whereas in pure gold only a single peak with $E = 0.80 \pm 0.04$ eV¹³ is reported. (7) The frequency factors for pure and alloyed copper and silver agree within the experimental error and are roughly $10^{15 \pm 0.8}$ cps. The frequency factors for Au-Mg and Au-Al, as summarized in Table VI, vary from 0.01 to about $10 \times 10^{15 \pm 0.08}$ cps.

One might summarize these experimental results with

the simple statement that alloying copper and silver with beryllium leaves the recovery spectrum of stages II and III completely unaltered in shape, activation energy, frequency factor, and order of kinetics, but a larger percent of the total initial damage introduced near absolute zero recovers in stage III in alloys than in the pure material at the expense of stage I. In alloyed gold, the shape, activation energy, and frequency factors are altered markedly; and also, as in copper and silver, stage III is enhanced at the expense of stage I.

From these experimental facts some conclusions about the type of defect responsible for stage-III recovery can be made. Of the three models discussed the present data indicates that the probable cause of stage III in copper and silver is long-range migration of vacancies and that stage II is due to correlated close-pair annihilation by vacancy migration. Although this model has the disadvantage that the observed activation energy of the stage-III defect, as obtained by radiation-damage experiments, is 10% to 15% lower than the vacancy migration energy, as determined in equilibrium and quenching experiments and compared in Table V, it seems to be more attractive than the two-interstitial model.

In gold no definite assignment can be given to the form of the defect migrating in stage III using only the results of the present experiment, but because of Venables and Balluffi's work and the effect of magnesium and aluminum on the recovery of gold, it is suggested that an interstitial is responsible for stage-III recovery.

ACKNOWLEDGMENTS

We would like to thank the Nuclear Radiation Laboratory under Professor J. S. Allen and Professor M. K. Brussel for the cyclotron irradiation. We would also like to thank C. Lee and D. Sims for their help in making measurements.

APPENDIX I. THE CORRECTION TIME

"Correction times" t' to the annealing time t result from the finite rise time of the temperature of the sample blocks T to the annealing temperature T_0 . The correction times are found by equating the change in resistivity at a temperature T to an equivalent change in resistivity at the bath temperature T_0 . This then gives an equivalent time t' in terms of the actual time t , the block temperature T , and the bath temperature T_0 .

$$\int \frac{d(\Delta\rho)}{(\Delta\rho)^n} = \frac{\sigma\nu A t'}{\delta^{n-1}} e^{-E/kT} = \frac{\sigma\nu_0 A_0 t}{\delta^{n-1}} e^{-E/kT_0}. \quad (\text{I.1})$$

Here it is assumed that $\sigma\nu A/\delta^{n-1}$ is approximately equal to $\sigma\nu_0 A_0/\delta^{n-1}$, so that solving for t' one obtains

$$t' = t \exp \left[-\frac{E}{k} \left(\frac{T_0 - T}{TT_0} \right) \right], \quad T_0 - T > 0. \quad (\text{I.2})$$

The temperature of the sample block is recorded continuously versus time, so that t , T , T_0 , and E are known quantities. In order to get t' , these curves are broken up into small intervals of Δt_i and the temperature at the center of the interval is used over the entire interval. This approximation becomes better as Δt_i becomes smaller. This procedure then yields a temperature-correction equation of the following form:

$$t' = \sum_{i=1}^N \Delta t_i' = \sum_{i=1}^N \Delta t_i \exp\left(-\frac{E}{k} \frac{T_0 - T_i}{T_0 T_i}\right). \quad (\text{I.3})$$

The activation energy is obtained roughly before the time corrections are applied, so that it may be used in Eq. (I.3) for the calculation of t' , leading to a more accurate determination of E .

APPENDIX II. THE RESISTANCE RATIO

In order to calculate the resistivity of solute A in base lattice B , the atomic percent x of the solute must be known and the resistance ratio r must be measured. The resistance ratio is defined as the ratio of the resistance at 0°C to the resistance at liquid-helium temperature, which is approximately 4.2°K . This ratio can be expressed using resistivities rather than resistances because the area factors, cross sectional area/length, cancel yielding the following equation:

$$r = (\rho_B + \rho_{\text{imp}} + \rho_A) / (\rho_{\text{imp}} + \rho_A). \quad (\text{II.1})$$

Here ρ_B , ρ_{imp} , and ρ_A are the resistivities of the base, background impurity, and desired solute atoms, respectively. The thermal components of the impurity terms at 0°C are neglected in the present paper. Using the fact that atomic percent of desired impurity x and the residual resistivity ρ are directly proportional, one has that

$$\rho = x\delta\rho. \quad (\text{II.2})$$

It is thus possible to calculate the resistivity of the known solute $\delta\rho$ in a particular base material. The resistivity per atomic percent of solute A in lattice B may be calculated, using Eqs. (II.1) and (II.2), to be the following:

$$\delta\rho = \rho_B / (r-1)x - \rho_{\text{imp}} / x. \quad (\text{II.3})$$

In the cases of beryllium and lithium in silver, the value of $\delta\rho$ is unknown, but using the assays given in Table I along with the experimental resistance ratios and Linde's data¹⁶ $\delta\rho$ can be calculated. The calculated values of $\delta\rho$ are given in Table II.

APPENDIX III. THE ACTIVATION ENERGY CALCULATED BY THE CHANGE-OF-SLOPE METHOD

In order to calculate the activation energy by using the change of slope method, the equation governing the migration of defects is needed. Equation (III.1) below describes n th order kinetics where Δc is the concentration of defects, σ is the number of atomic sites around a defect within which the migrating defect is certain to be annihilated, ν is the frequency factor, A the entropy sector, E the activation energy for migration, T the absolute temperature, and k Boltzmann's constant,

$$d(\Delta c)/dt = (\sigma\nu A)(\Delta c)^n e^{-E/kT}. \quad (\text{III.1})$$

If the resistivity decrease associated with the annihilation is δ , then the resistivity will obey the following equation:

$$\frac{d(\Delta\rho)}{dt} = \frac{(\sigma\rho A)(\Delta\rho)^n}{\delta^{n-1}} e^{-E/kT}. \quad (\text{III.2})$$

Now taking the ratio of Eq. (III.2) at two temperatures one obtains Eq. (III.3):

$$\frac{d(\Delta\rho)/dt|_{T_1}}{d(\Delta\rho)/dt|_{T_2}} = \frac{(\Delta\rho)_{T_1}^n}{(\Delta\rho)_{T_2}^n} \exp\left[-\frac{E}{k}\left(\frac{T_2 - T_1}{T_2 T_1}\right)\right], \quad T_2 > T_1. \quad (\text{III.3})$$

Here it has been assumed that σ and δ are not temperature-dependent and that νA is effectively constant over the temperature region of interest. If the annealing rates $d(\Delta\rho)/dt$ are compared at the moment when the specimen is removed from T_1 and started at T_2 then $\Delta\rho_{T_1} = \Delta\rho_{T_2}$. Also note that the rates $d(\Delta\rho)/dt|_{T_1}$ and $d(\Delta\rho)/dt|_{T_2}$ are simply the slope m_1 at the end of the isothermal at T_1 and the slope m_2 at the beginning of the isothermal at T_2 . Solving for E one then obtains Eq. (III.4) for the activation energy E ,

$$E = (kT_2 T_1 / (T_2 - T_1)) \ln(m_2/m_1), \quad T_2 > T_1, \quad m_2 > m_1. \quad (\text{III.4})$$

If one thus plots the isothermals and takes the proper slopes, the activation energy between T_1 and T_2 can be obtained. It is obvious that as T_1 approaches T_2 the assumptions regarding ν and A become better and E becomes more representative of the energy between T_1 and T_2 . Note that this development requires that there be only one singly activated process occurring between T_1 and T_2 .